

Obesity-induced TET2 dysfunction in DNMT3A mutated haematopoietic cells increases myelopoiesis, resulting in increased risk for cardiovascular disease development

A THESIS IS SUBMITTED TO HAN UNIVERSITY OF APPLIED SCIENCE FOR THE
DEGREE OF BACHELOR OF LIFE SCIENCE

ARINA KOCHETKOVA (1634642)

BAKER HEART AND DIABETES INSTITUTE
HAEMATOPOIESIS AND LEUKOCYTE BIOLOGY LABORATORY

SUPREVISORS:

PROF. ANDREW MURPHY

DR. MAN KIT SAM LEE

Submission date: 13/06/2023

Table of Content

| | |
|--|-----------|
| Abstract | 3 |
| Abbreviations | 5 |
| Introduction | 6 |
| 1. CHIP: definition and risk factors..... | 6 |
| 2. CHIP as a risk factor for malignancy and CVD | 6 |
| 3. DNMT3A and TET2..... | 7 |
| 4. Mutations in DNMT3A and TET2 as drivers of CVD..... | 8 |
| 5. Obesity promotes CHIP progression..... | 9 |
| Materials and methods | 11 |
| 1. Mice maintenance and treatments..... | 13 |
| 2. Competitive Bone Marrow Transplantation (BMT)..... | 13 |
| 3. EchoMRI | 13 |
| 5. Leukocyte measurements | 14 |
| 5.1 Blood samples preparation..... | 14 |
| 5.2 Bone marrow samples preparation | 14 |
| 5.1 Liver samples preparation | 14 |
| 5.1 Flow cytometry | 14 |
| 6. cKit ⁺ cell sorting | 15 |
| 7. TET2 functional assay..... | 15 |
| 8. Liver tissue analysis..... | 15 |
| 9. Statistical analysis | 15 |
| Results | 16 |
| 1. <i>DNMT3A</i> ^{+/<i>R878H</i>} mutation further increases body weight and fat content when fed a HFD | 16 |
| 2. High fat diet accelerates myelopoiesis in WT/ <i>DNMT3A</i> ^{+/<i>R878H</i>} mice | 16 |
| 3. High fat diet accelerates liver fat and macrophage content in WT/ <i>DNMT3A</i> ^{+/<i>R878H</i>} mice .. | 17 |
| 4. Obesity reduces TET2 activity in bone marrow HSCs | 18 |
| 5. AMPK activator O-304 reduced reduces HFD induced body and fat mass, and blood monocytes..... | 19 |
| Discussion | 21 |
| Conclusion | 22 |
| References | 23 |
| Appendix | 26 |

| | |
|-----------------------------|----|
| Supplementary table | 26 |
| Supplementary figures | 27 |

Abstract

Clonal haematopoiesis of intermediate potential (CHIP) driven by somatic mutations in *DNMT3A* and *TET2* has been recently recognized as a new risk factor for cardiovascular diseases (CVD). The haematopoietic clones with mutations in these genes are frequently found in myeloid malignancies and according to preclinical data, patients with progressive CHIP usually exhibit a dual loss of DNMT3A and TET2. Both DNMT3A and TET2 are important epigenetic modifiers that control the balance between self-renewal and differentiation in haematopoietic stem cells (HSCs). In the context of CVD, the deficiency of either DNMT3A or TET2 results in the increased production of myeloid cells that in its turn contribute to the formation of atherosclerotic plaques. The skewing of haematopoiesis towards myeloid lineage is the result of both inadequate epigenetic regulation in HSCs as well as an increased inflammatory response in already differentiated cells. Obesity is a multifactorial energy balance disorder characterized by adipose tissue expansion and low-grade inflammation. Multiple metabolic regulators become downregulated in obesity conditions and adenosine monophosphate (AMP)-activated protein kinase (AMPK) belongs to this group. AMPK is importantly involved in homeostasis maintenance including the regulation of TET2 activity in HSCs. As shown by previous studies, the AMPK-TET2 axis in HSCs is indeed commonly downregulated in obesity, thus increasing the risk for CVD. Our laboratory previously established that diabetes-induced TET2 dysfunction in HSCs promoted DNMT3A-driven CHIP and that AMPK activators managed to reverse this process. Therefore, in the current study, we first aimed to investigate if obesity-induced TET2 dysfunction is capable of accelerating the outgrowth of DNMT3A clones towards a myeloid lineage and, secondly, to explore if this process can be reversed by the activation of AMPK. For the first aim, CD45.1 recipient mice were irradiated and transplanted with the donor bone marrow (BM) cells consisting of 90% CD45.1 WT and either 10% CD45.2 *DNMT3A*^{+/+} (control) or 10% CD45.2 *DNMT3A*^{+/*R878H*} (*DNMT3A* CHIP). After the 8-week recovery period of the immune system of either 90% WT/10% *DNMT3A*^{+/+} or 90% WT/10% *DNMT3A*^{+/*R878H*} cells, both groups were introduced with a chow or high-fat diet (HFD) for 16 weeks. Using flow cytometry, we found that diet-induced obesity increased monocyte levels in blood regardless of *DNMT3A* mutation, however, *DNMT3A* mutation was seen to further accelerate monocytosis in obese mice. In addition, we tracked mice body composition with EchoMRI every 4 weeks and observed that obesity caused an overall body weight and fat mass increase. After the 16-week period, mice were euthanized, and the bone marrow and liver samples were harvested. We established an increased abundance of HSCs and myeloid precursors common myeloid progenitors (CMPs) and granulocyte-monocyte progenitors (GMPs) in *DNMT3A* CHIP mice, which was evidence of accelerated myelopoiesis. Liver samples were analysed for macrophage levels and lipid content by flow cytometry and liver tissue sectioning and staining, respectively, and we observed that obesity-driven inflammation was aggravated by the *DNMT3A*^{+/*R878H*} phenotype. To establish if obesity-induced myelopoiesis is driven by TET2 dysfunction, we profiled BM HSCs on 5-hmC status and indeed found dramatically decreased 5-hmC levels in both obese groups. For the second aim, CD45.1 recipient mice were transplanted with donor BM cells of 90% CD45.1 WT and 10% CD45.2 *DNMT3A*^{+/*R878H*} and after recovery, mice were placed on a HFD with or without AMPK activator O-304 for 16 weeks. As this study is still ongoing, we have not yet observed changes in blood monocyte levels at the 8-week timepoint, however, O-304 did reduce body weight and fat mass accumulation. Collectively, this data shows that diet-induced obesity further exacerbates

myelopoiesis of HSCs presumably by suppressing TET2 in *DNMT3A* mutant mice. It is still to be investigated if AMPK activation by O-304 is capable to reverse the process and inhibit obesity-promoted exacerbated myelopoiesis.

Keywords: DNMT3A, TET2, obesity, CVD, CHIP, AMPK

Abbreviations

| | |
|-------------------------------|---|
| 5-hmC | 5-hydroxymethylcytosine |
| 5-mC | 5-methylcytosine |
| AML | Acute Myeloid Leukemia |
| AMPK | 5' Adenosine Monophosphate-activated Protein Kinase |
| AMPER | Alfred Medical Research Education Precinct |
| BM | Bone Marrow |
| BMT | Bone Marrow Transplantation |
| CHIP | Clonal Haematopoiesis of Intermediate Potential |
| CMP | Common Myeloid Progenitor |
| CVD | Cardiovascular disease |
| Cxcl1/2 | CXC chemokine ligands 1/2 |
| DNMT3A | DNA methyltransferase 3A |
| EDTA | Ethylenediaminetetraacetic Acid |
| FACS | Fluorescent-activated Cell Sorting |
| FCS | Fetal Calf Serum |
| FSC-A | Forward Scatter Area |
| gDNA | Genomic DNA |
| GMP | Granulocyte Monocyte Progenitor |
| HFD | High Fat Diet |
| HSPC | Haematopoietic Progenitor Stem Cells |
| HSC | Haematopoietic Stem Cells |
| IL-1β | Interleukin-1 β |
| MDS | Myelodysplastic Syndrome |
| NLRP3 | NLR family pyrin domain containing 3 |
| PAMP | Pathogen-associated Molecular Patterns |
| PBS | Phosphate-buffered Saline |
| PRR | Pattern Recognition Receptors |
| SSC-A | Side Scatter Area |
| SSC-H | Side Scatter Height |
| TET2 | Ten-eleven Translocation-2 |
| TBRS | Tatton-brown Rahman syndrome |
| WT | Wild Type |

Introduction

Cancer and cardiovascular disease (CVD) remain two major causes of death worldwide and the susceptibility to both disorders increases with aging. Age-related diseases associate with the elevated incidence of somatic mutations in haematopoietic stem cells in various tissues and the risk for this arises from the cumulative effect of the natural aging process as well as from exposure to external mutagenic factors^{1,2}. The accumulation of mutated cell clones, established as a driving force in carcinogenesis, has recently been recognized as an important risk factor in CVD development⁵.

1. CHIP: definition and risk factors

The haematopoietic system is one of the most rapidly dividing tissues, meaning that the incidence of somatic mutation in haematopoietic cells is rather high⁵. Certain mutations obtained by haematopoietic stem cells (HSCs), provide them a competitive advantage among non-mutant cells, allowing the outgrowth of hematopoietic clones. The mutant progeny of HSCs maintains the ability to differentiate and thus is detectable in peripheral blood^{2,4}. The process when a single mutation occurs in $\geq 2\%$ of HSCs is defined as clonal hematopoiesis of indeterminate potential (CHIP). Importantly, the risk of developing CHIP-initiated hematological malignancies is low, however, individuals with CHIP have a substantially increased susceptibility to non-hematological diseases such as CVD and type 2 diabetes³.

The accumulation of haematopoietic clones becomes common with aging so that by the age of 70, approximately 10-20% of healthy individuals obtain the clones with at least 2% of mutated alleles^{1,2,4}. On the molecular level, aging implies an easier acquisition of somatic mutation due to the downregulation of the DNA repairing system, telomeres shortening and an increasing degree of chronic low-grade inflammation recently termed as inflammaging^{1,4,6}. Despite these processes occurring naturally with time, they may be substantially accelerated by continuous exposure to age-dependent mutational processes. The exogenous stressors such as radiation, air pollutants, tobacco smoking, and diet significantly interfere with cellular homeostasis and thus may promote premature aging, increasing the tendency of retaining somatic mutations^{1,4,7}.

2. CHIP as a risk factor for malignancy and CVD

CHIP is classified as a haematological pre-malignant state and therefore has the potential to progress into various haematological cancers such as myelodysplastic syndromes (MDS) or acute myeloid leukemia (AML)⁸. However, the rate of overt neoplasia development in individuals with CHIP is approximately 0.5%-1% per year, meaning that the majority of patients remain asymptomatic⁹. As shown by previous studies, the risk of malignant transformations directly correlates with the number of somatic mutations and is rapidly increased in individuals who possess 10% or more of mutated HSCs¹⁰.

Although the risk of CHIP progression into hematological diseases is rather low, the all-cause mortality rate is significantly higher for individuals harboring hematopoietic clones. Interestingly, patients with CHIP-associated mutations were shown to be more susceptible to death from CVD rather than hematological cancer¹⁰. A recent clinical study demonstrated that 60% of elderly patients with atherosclerosis have either no or only one conventional CVD-related risk factor such as hyperlipidemia or diabetes, suggesting that there is a range of asymptomatic age-dependent CVD risk factors that are yet to be identified²⁰.

According to recent studies, approximately 20 genes are implicated in CHIP development, however, in the majority of cases CHIP is initiated with mutations in a specific group of genes including ten-eleven translocation-2 (*TET2*) and DNA methyltransferase 3A (*DNMT3A*)^{5,9}. Both genes encode epigenetic modifiers and are known as leukemia-driver genes and have previously been shown to be associated with an increased risk of CVD^{2,9,11}.

3. *DNMT3A and TET2*

HSCs residing in the bone marrow (BM) are determined by their ability to replenish the haematopoietic system throughout its lifetime. This is achieved by their differentiation into specific cell types as well as their continuous self-renewal capacity¹². The balance between differentiation and self-renewal of HSCs is controlled by both intrinsic factors such as epigenetic modifications and transcription factors, and extrinsic factors such as growth factors and cytokines which all together regulate gene expression and thus determine cell fate¹³. As HSCs are yet to be differentiated, their chromatin is in a quiescent state which makes cells susceptible to any shifts in epigenetic regulations¹⁴. DNA 5-cytosine methylation and hydroxymethylation are some of the major epigenetic modifications in HSCs that are catalyzed by DNA methyltransferase 3A (*DNMT3A*) and ten-eleven translocation 2 (*TET2*), respectively¹³. By adjusting the methylation status of DNA, the enzymes regulate the chromatin accessibility to transcription factors, therefore either activating or repressing the expression of particular genes including those that control differentiation and self-renewal of HSCs¹⁴.

DNMT3A enzyme belongs to a family of DNA methyltransferases that is responsible for the introduction of the methyl group to 5-cytosine residue on DNA (5-mC)^{5,12}. *TET2* is a member of the family of dioxygenases that catalyzes the passive DNA demethylation through the oxidation of 5-methylcytosine to 5-hydroxymethylcytosine (5-hmC) (**Figure 1**)¹⁶. Although *DNMT3A* and *TET2* perform the antagonistic roles of adding and removing a methyl group, loss-of-function mutations in any of the enzymes lead to paradoxically similar clinical outcomes, suggesting that both proteins function in parallel to ensure a single end result¹⁵. As confirmed by previous studies, the ablation of *DNMT3A* and the resulting global loss of DNA methylation in HSCs leads to the reduction of differentiation capacity and increased self-renewal^{12,15}. *TET2* dysfunction and therefore insufficient hydroxymethylation was similarly associated with aberrant HSC self-renewal and, in addition, with skewing haematopoiesis towards the myeloid lineage, known as myelopoiesis^{15,18,19}.

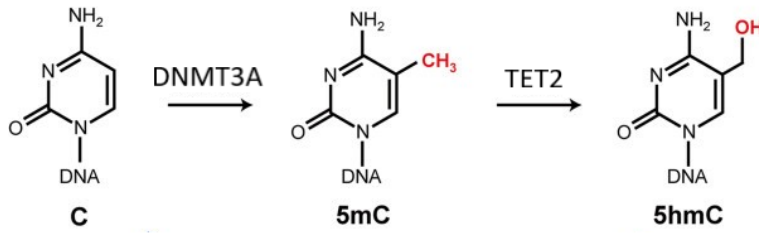


Figure 1. The schematic representation of DNA methylation and hydroxymethylation. The methylation of the cytosine residue (C) on DNA is performed by DNMT3A and a methyl group (CH₃) is added to the 5th position on the pyrimidine ring to form 5-methylcytosine (5mC). TET2 catalyzes the oxidation of the 5mC by adding a hydroxyl group to the 5-methyl group, forming 5-hydroxymethylcytosine (5hmC).

4. Mutations in DNMT3A and TET2 as drivers of CVD

Mutations in both *DNMT3A* and *TET2* are frequently found in individuals with age-associated CHIP as well as in hematological malignancies^{15,16,17}. As recently reported, *DNMT3A* and *TET2* exhibited the highest mutation rate among all CHIP-associated genes and in 10-20% of individuals with AML either DNMT3A or TET2 is dysfunctional^{12,19}. However, as previously stated, for patients with CHIP, the risk of developing cancer is much lower than the chance of experiencing a cardiometabolic disease such as myocardial infarction or heart failure^{2,10}.

There is a number of studies that demonstrate the direct link between the decreased function of DNMT3A and elevated incidence of cardiovascular events⁴. The loss of DNMT3A in mice was seen to increase the self-renewal capacity of HSCs in the BM and progressively reduce their differentiation potential^{21,22}. Although DNMT3A deficiency in HSCs has been clearly shown to increase the risk for cardiac dysfunction, the exact mechanism of how it acts to initiate CVD is yet to be discovered²³. In myeloid cell lines, however, the downstream consequences of DNMT3A loss were recently demonstrated by Sano and colleagues. The research group revealed that the DNMT3A deficiency in myeloid cells promotes an inflammatory response by upregulating CXC chemokine ligands 1/2 (Cxcl1/Cxcl2), that are secreted in response to pathogen-associated molecular patterns (PAMPs) in non-mutant cells²⁴. Cxcl1 and Cxcl2 are chemoattractants that recruit neutrophils to the site of inflammation including damaged endothelial cells, where neutrophils are capable of infiltrating the vessel walls and initiating atherosclerotic plaque formation²⁵.

Mutated *TET2* was similarly seen to be associated with an increased risk of CVD⁴. Low enzymatic activity of TET2 and thus the deficiency of 5-hmC in mice results in aberrant hematopoiesis skewed largely towards the production of myeloid cells such as monocytes and neutrophils. The oversupply of inflammatory myeloid cells is the main driver of atherosclerotic disease progression in diabetic and hypercholesterolemic mice. Increased blood monocytes are known to fuel atherosclerotic lesion formation and progression as they infiltrate vascular walls whereas neutrophils facilitate further differentiation of HSCs into the myeloid lineage as well as infiltrate the plaques at the later stages of CVD^{26,27}. For CHIP patients without progressive metabolic diseases, however, the consequences of *TET2* mutation described by Fuster are more common. The study revealed that TET2-deficient macrophages exhibit an increased secretion of

proatherogenic interleukin-1 beta (IL-1 β), mediated by NLR family pyrin domain containing 3 (NLRP3) inflammasome. IL-1 β is a proinflammatory cytokine secreted in response to PAMPs in *TET2* non-mutant mice to initiate an inflammatory reaction at the sites of infection. However, the excess of IL-1 β was seen to activate endothelial cells as well as directly accelerate myeloid cell production in the BM which further results in endothelium infiltration by monocytes and neutrophils and therefore atherosclerotic plaque formation²⁰.

5. Obesity promotes CHIP progression

The risk of CVD development increases with age, and besides CHIP, this association may be enhanced by metabolic disorders including obesity. Obesity is a multifactorial disease with a complex of pathogenetic dysregulations in cellular mechanisms that lead to adverse health outcomes. Approximately 39-49% of the world's population have recently reported being overweight, and this number continues to increase annually²⁸. Obesity-associated chronic inflammation is the major driver of other non-resolving inflammatory conditions such as insulin resistance, metabolic syndrome, and atherosclerosis^{29,30}. The link between obesity and DNMT3A-driven CHIP was described in a study by Deuren's group. They demonstrated that approximately 20% of middle-aged individuals who were overweight develop haematopoietic clones including those with *DNMT3A* mutations that are linked to cardiovascular and metabolic diseases. The accelerated clone growth was mainly associated with insulin resistance and the deficiency of high-density lipoprotein cholesterol, suggesting that the inflammatory environment created by these conditions sustains further progression of DNMT3A-driven CHIP³².

Besides this, an excessive increase of adipose tissue in a body, or adiposity, was shown to enhance myeloid cell production, which plays an important role in CVD progression^{29,31}. Nagareddy's group was the first to define the regulatory mechanism between an inflamed adipose tissue and BM cells, where IL-1 β was clearly placed as a systemic hormone able to induce an aberrant myelopoiesis in response to inflammation³⁰. Their study established that inflammatory cytokines secreted by adipocytes are local stimulants of macrophage pathogen recognition receptors (PRR), and their activation results in the upregulation of IL-1 β expression and secretion. As previously mentioned, excessive levels of IL-1 β provoke atherosclerosis development by directly increasing myelopoiesis in the BM^{29,30}.

Another link between adiposity and myelopoiesis was demonstrated to be through overnutrition where fatty acids and glucose and inflammation were capable to suppress the function of 5'-adenosine monophosphate protein kinase (AMPK)^{33,34}. AMPK is a key player in maintaining cellular energy homeostasis and participates in multiple metabolic pathways including TET2 5-hmC axis regulation. By acting as an upstream TET2 stabilizer, AMPK ensures sufficient TET2 activity and thus adequate levels of 5-hmC, which are crucial for balanced haematopoiesis^{35,36}. Wu and colleagues demonstrated a direct role of increased glucose, or hyperglycemia, in promoting exacerbated myelopoiesis through reducing AMPK activity and destabilizing TET2 (Figure 2)³⁶.

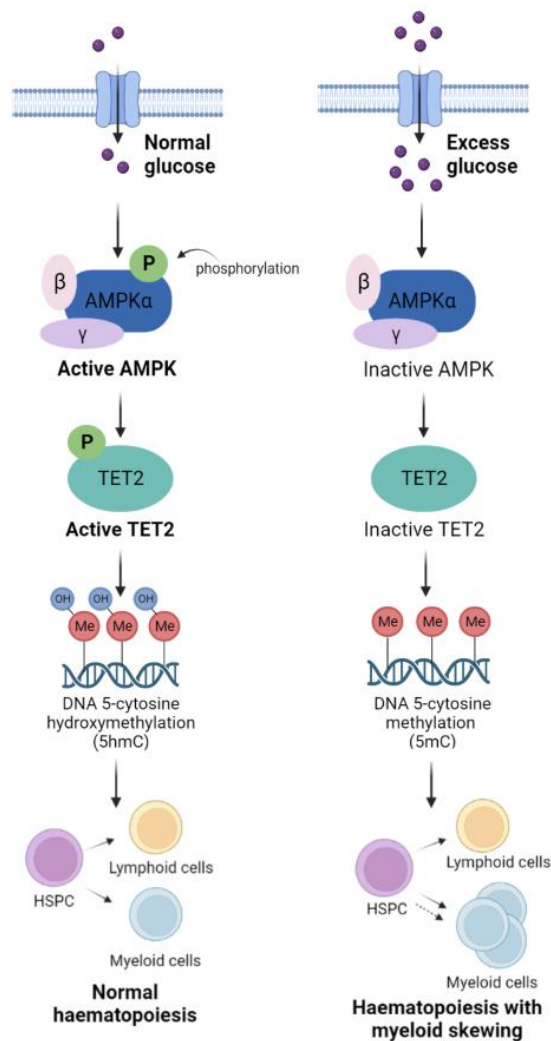


Figure 2. The schematic overview of AMPK-TET2 pathway in normal and diabetic conditions. In a normal glucose state, AMPK is phosphorylated at active sites and thus represents normal activity; AMPK phosphorylates and activates TET2 which ensures DNA hydroxymethylation at 5' cytosine end (5-hmC); sufficient 5-hmC levels contribute to keeping haematopoiesis balance. The excess glucose suppresses AMPK activation leading to impaired AMPK functioning; AMPK is incapable to phosphorylate TET2 which therefore becomes unstable and unable to maintain normal 5-hmC status; insufficient 5-hmC results in imbalanced haematopoiesis skewed towards myeloid lineage.

Our laboratory has previously reported that in the scenario CHIP, diabetes-induced TET2 dysfunction in BM HSCs accelerated DNMT3A myeloid clonal outgrowth, which was prevented by activating AMPK (unpublished data). This study represented, that HSCs carrying *DNMT3A* mutation were subjected to myeloid skewing, and diabetes further exacerbated the myelopoiesis of *DNMT3A* mutant HSCs by suppressing the AMPK-TET2 pathway, however, the introduction of the AMPK activator partially restored the haematopoietic balance. Although obesity was shown to promote DNMT3A clonal expansion, the exact pathway of how it occurs is yet to be discovered. Therefore, the goal of the current research is to investigate the link between obesity-driven TET2 dysfunction and DNMT3A myeloid clonal expansion as well as to explore if the AMPK activator is capable of restricting the progression of DNMT3A-driven CHIP. We hypothesize that obesity will exacerbate myelopoiesis via dysregulation of AMPK and TET2 activity and that activation of AMPK will suppress this process.

Materials and Methods

Two cohorts were used to investigate the role of a HFD on DNMT3A-mutated myelopoiesis. To mimic the scenario of CHIP, in the first cohort, irradiated CD45.1 recipient mice were transplanted with 90% donor CD45.1 wild type (WT) and either 10% donor CD45.2 *DNMT3A^{+/+}* or 10% donor CD45.2 *DNMT3A^{+R878H}* BM cells. Mice were then left for 8 weeks to reconstitute the entire immune system of either 90% WT/10% *DNMT3A^{+/+}* or 90% WT/10% *DNMT3A^{+R878H}* cells. After 8 weeks, both groups were fed either a normal chow or high-fat diet (HFD) for 16 weeks (**Figure 3A**). In the second cohort, a similar approach was performed, however, irradiated CD45.1 recipient mice were transplanted with 90% donor CD45.1 WT and only 10% donor CD45.2 *DNMT3A^{+R878H}* BM cells. After 8 weeks of reconstitution, mice were fed a HFD with or without 1% AMPK activator (O-304) in their diet for 16 weeks (**Figure 3B**).

For both cohorts, their body composition consisting of fat and lean mass was measured using an EchoMRI every 4 weeks. To explore if the diet was affecting myelopoiesis, blood samples were collected via tail vein bleeding every 4 weeks and the percentages of monocytes were determined. To further confirm that myelopoiesis was occurring, mice were humanely euthanized after 16 weeks of diet and their BM was harvested to measure the abundance of monocyte precursor cells such as HSCs, common-myeloid progenitors (CMPs) and granulocyte monocyte progenitors (GMPs). The liver was also collected to assess liver macrophage and fat content. All experiments that involved leukocyte analysis were conducted using flow cytometry. The liver fat content assessment was performed by preparing and further imaging liver tissue slides (**Figure 3C**). Unfortunately, due to time constraints, the second cohort has not completed its 16 weeks of feeding period and therefore, only EchoMRI and blood monocyte data were captured.

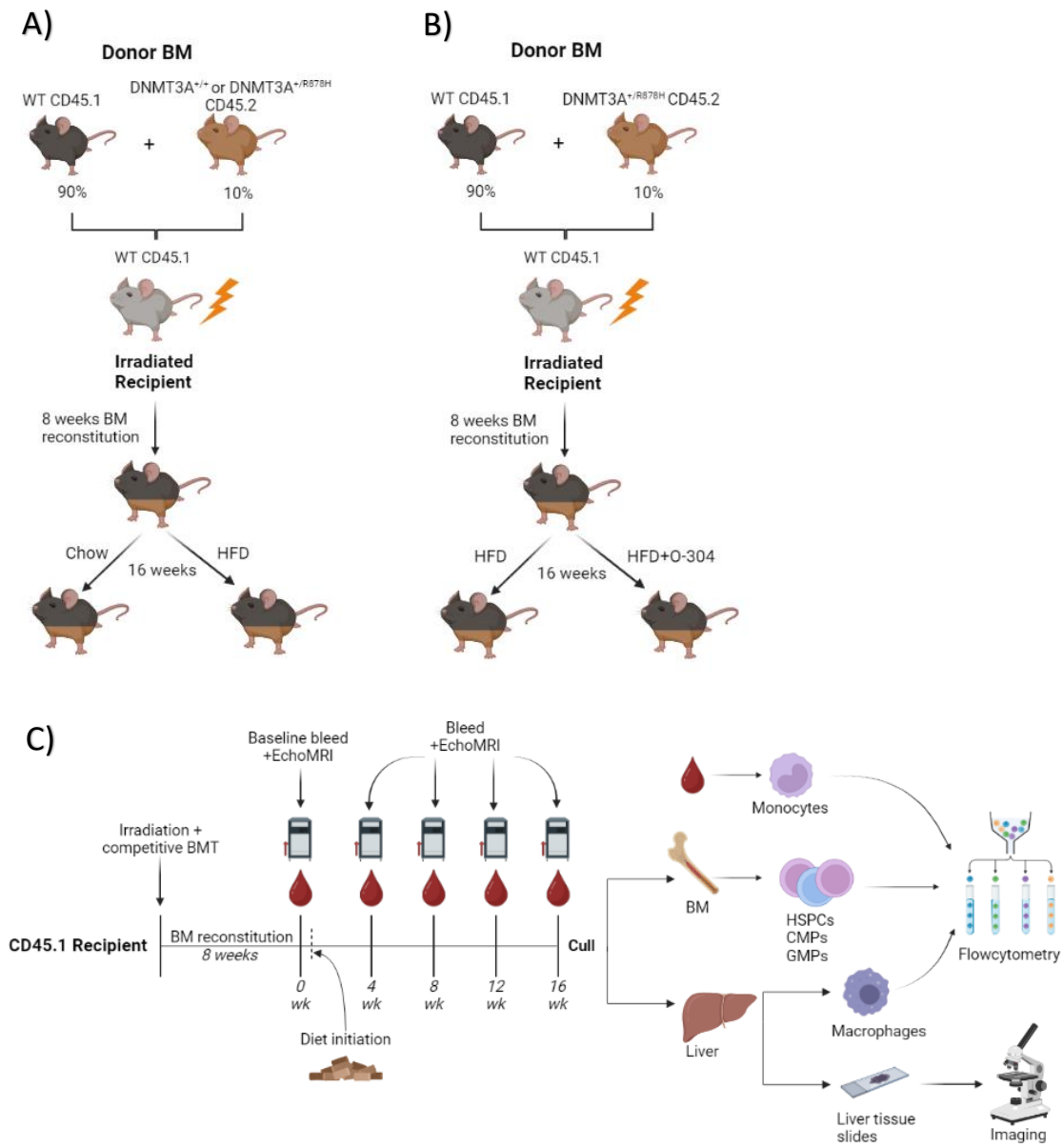


Figure 3. Overview of the experimental plan. The experimental setup used for the first cohort: the donor bone marrow (BM) is mixed in the proportion of 90% CD45.1 WT + 10% CD45.2 DNMT3A^{+/+} for the control group and 90% CD45.1 WT + 10% CD45.2 DNMT3A^{+/R878H} for the DNMT3A CHIP group and transplanted into the CD45.1 irradiated recipients. After 8 weeks of reconstitution (recovery), the control and DNMT3A CHIP groups are subjected to a normal chow or high-fat diet (HFD). B) The experimental setup used for the second cohort: the donor bone marrow (BM) is mixed in the proportion of 90% CD45.1 WT + 10% CD45.2 DNMT3A^{+/R878H} and transplanted into the CD45.1 irradiated recipients. After 8 weeks of reconstitution (recovery), the control and mutant group are put on HFD with or without supplementation of AMPK activator O-304. C) The workflow scheme: recipient CD45.1 mice are irradiated, injected with donor BM (of a certain mixture), and allowed to reconstitute for 8 weeks. When mice are fully recovered (week 0), the baseline bleed and EchoMRI data are collected and afterward mice are fed a certain diet for 16 weeks. Blood collection through tail vein bleed and EchoMRI are done every 4 weeks until mice are humanely euthanized at week 16. Blood is analysed on monocyte percentage whereas EchoMRI was used to examine the body composition of mice. After euthanasia, the BM is harvested and the percentages of haematopoietic stem cells (HSCs), common myeloid progenitors (CMPs), and granulocyte-monocyte progenitors (GMPs) are measured. Liver samples are collected and analysed on macrophage content and liver tissue slides are stained and analysed on fat content by imaging. The experiments involved BM and blood cell measuring were conducted using flow cytometry.

1. Mice maintenance and treatments

The study was approved by the animal ethics committees (AEC) under the AEC-approved project number P2039 at the Alfred Medical Research Education Precinct (AMREP). Male wild-type CD45.1 mice were bred at the AMREP animal facility. Male CD45.2 *DNMT3A*^{+/+} and CD45.2 *DNMT3A*^{+/*R878H*} mice were provided by Marco Herold's laboratory at the WEHI using CRISPR technology. Mice were housed at the AMREP animal facility in a standard light/dark cycle and given access to food and water on an ad libitum basis. For the first cohort, both WT/*DNMT3A*^{+/+} and WT/*DNMT3A*^{+/*R878H*} groups were kept on either a normal chow diet or a high-fat diet (HFD; 60% kcal) to initiate diet-induced obesity (DIO). For the second cohort, WT/*DNMT3A*^{+/*R878H*} mice were placed on HFD with or without additional supplementation of the AMPK activator O-304. All diets were purchased from Specialty Feeds (WA, Australia).

2. Competitive Bone Marrow Transplantation (BMT)

Competitive bone marrow transplantation (BMT) implies the transfer of the BM donor control CD45.1 cells and target CD45.2 cells into the same recipient to allow to measure the competitive advantage of the target CD45.2 population against the control CD45.1. Donors CD45.1 WT and CD45.2 *DNMT3A*^{+/+} and CD45.2 *DNMT3A*^{+/*R878H*} were euthanized and both tibias and femurs of each mouse were collected and cleaned by taking off muscles and connective tissues. BM cells were flushed through a 40µM filter into a 50mL falcon tube with a syringe filled with phosphate-buffered saline (PBS) without Mg²⁺/Ca²⁺. After flushing, BM cells were counted using an XS-1000i Systemic Hematology Analyser. Cells were then centrifuged at 1000rpm for 10 mins at 4°C and cell pellets were resuspended in BMT media to a final concentration of 1.2-2*10⁷ cells/ml. BMT media was prepared with RPMI 1640 media supplemented with 2% fetal calf serum (FCS), 0.5% penicillin-streptomycin (pen-strep), and 0.5µl/ml heparin. For the first cohort, the final BMT injections were prepared by mixing 90% of CD45.1 WT cells with 10% of CD45.2 *DNMT3A*^{+/+} cells for the control group (WT/*DNMT3A*^{+/+}) and 90% of CD45.1 WT cells with 10% of CD45.2 *DNMT3A*^{+/*R878H*} cells for the mutant group (WT/*DNMT3A*^{+/*R878H*}). For the second cohort, only the WT/*DNMT3A*^{+/*R878H*} BMT injections were prepared using the same proportions of cells.

Recipient CD45.1 mice were irradiated (2x 550rads, 4 hours apart) and subjected to BMT by intravenous (I.V.) injections with the donor BM mixture the next day. To inject recipient mice with donor BM, mice were placed in a mice holder and 200 µl of donor BM mixture cells were injected via the tail vein. Recipient CD45.1 WT mice were supplied with antibiotics, namely neomycin and polymyxin B (10µg/ml in 500ml bottle) 2 weeks after the BMT. During the 8-week reconstitution (recovery) period, mice were fed a standard chow diet and supplied with additional mash (wet standard chow diet) daily. Mash was introduced to ensure that mice were sufficiently fed. From the total 8-week period reconstitution, mice were first monitored and weighed daily for 3 weeks and then weekly for the remaining 5 weeks.

3. EchoMRI

Mouse body composition (fat mass and lean body mass) was measured monthly with a 4-in-1 EchoMRI body composition analyzer (Colombus Instruments). To perform the analysis, mice were inserted into a cylinder holder and physically restrained to prevent any movement. The cylinder containing the mouse

was then inserted into the EchoMRI machine for body composition analysis. The total body mass of mice was measured using laboratory scales. All the data were analysed using GraphPad Prism.

4. Leukocyte measurements

4.1 Blood samples preparation

Blood samples of 75µL were collected via tail vein bleeding into a 0.5mL Epi-tube containing 5µL of 0.5M ethylenediaminetetraacetic acid (EDTA) to prevent blood clotting. Samples were mixed with 7mL of 1X RBC Lysis Buffer (BD pharm Lyse; BD biosciences) and incubated at RT for 15 minutes to lyse red blood cells. After 15 minutes, samples were centrifuged at 3000 rpm for 5 minutes at 4°C before cell pellets were resuspended in 200µL of flow-activated cell sorting (FACS) buffer (containing 1x Hank's Balanced Salt Solution without Ca²⁺ and Mg²⁺, with 0.1% w/v Bovine Serum Albumin and 5mM EDTA) ready to be stained for flow cytometry.

4.2 Bone marrow samples preparation

Following euthanasia, both tibias and femurs of each mouse were collected and cleaned by taking off muscles and connective tissues. All BM cells were flushed with phosphate-buffered saline (PBS) without Mg²⁺/Ca²⁺ through a 40µm filter. Samples were lysed in 1mL of 1x RBC Lysis Buffer for 5 minutes. After 5 minutes, cells were centrifuged at 3000rpm for 5 minutes at 4°C and resuspended in 200µL FACS buffer ready to be stained for flow cytometry.

4.3 Liver samples preparation

Following euthanasia, livers were dissected from mice and mashed through a 40µm cell strainer with PBS without Mg²⁺/Ca²⁺ to obtain a single-cell suspension. Samples were lysed with 7mL of 1X RBC Lysis Buffer for 15 mins and then centrifuged at 3000rpm for 5 minutes at 4°C. Cells were resuspended in FACS buffer ready to be stained for flow cytometry.

4.4 Flow cytometry

Blood samples were stained with a combination of antibodies against PE/Cy7-CD45.1, AF700-CD45.2, PerCP/Cy5.5-Gr-1, BV605-CD115, PE-CD3, FITC-CD8, BUV469-CD4, APC-B220 at a dilution of 1:400 and then incubated for 30 minutes in the dark on ice. Flow antibody details can be found in Table S1. The stained samples were washed with 500µL of FACS Buffer, centrifuged at 3000rpm for 2.5 minutes, and resuspended in 200µL of FACS Buffer. After being transferred into FACS tubes, samples were acquired with BD LSR Fortessa (BD Biosciences) flow cytometer using the FACSDiva software. Data were analyzed with FlowJo Software (TreeStar). As shown in **Figure S1**, the cells for analysis were determined on the graph of side scatter area (SSC-A) vs. forward scatter area (FSC-A), and single cells were identified using SSC-A vs. SSC-height (SSC-H) to exclude doublets. From the single-cell population, monocytes were identified as CD45⁺CD115⁺ and later divided into CD45.1⁺ and CD45.2⁺ populations.

Bone marrow samples were stained against lineage committed lineage-committed cells (FITC-CD2, FITC-CD19, FITC-TER119, FITC-Gr-1, FITC-B220, FITC-CD3, FITC-CD4, FITC-CD11b), stem cell surface markers (PB-Sca1, APC/Cy7-cKit, PerCP-Fcy, and APC-CD34) and CD45 markers (PE/Cy7-CD45.1 and AF-CD45.2) for 30 minutes in the dark on ice. Stained cells were washed with 500µL FACS buffer and centrifuged at 3000 rpm for 5 minutes. Samples were then transferred into FACS tubes and immediately acquired using a BD LSR Fortessa (BD Biosciences) flow cytometer. As

shown in **Figure S2**, HSCs were identified as Lin⁻Sca1⁻cKit⁺. From the HSPC population, CMPs and GMPs were distinguished as Lin⁻Sca1⁺cKit⁺Fcy^{int}CD34^{int} and Lin⁻Sca1⁺cKit⁺Fcy^{hi}CD34^{hi} respectively. HSCs, CMPs, and GMPs were further divided into CD45.1⁺ and CD45.2⁺ populations. Data were analyzed using FlowJo Software.

Liver macrophages were stained with a combination of antibodies against FITC-CD11b, PE/Cy7-F480, PE/Cy7-CD45.1, and AF-CD45.2. Liver macrophages were identified as CD11b⁺F480⁺ and distinguished between CD45.1⁺ and CD45.2⁺.

5. cKit⁺ cell sorting

For cKit⁺ fluorescent-activated cell sorting (FACS), samples were stained against lineage-committed cells (FITC-CD2, FITC-CD19, FITC-TER119, FITC-Gr-1, FITC-B220, FITC-CD3, FITC-CD4, FITC-CD11b) and incubated for 30 minutes on ice in dark since the cKit⁺ enrichment yields only ~40% cKit⁺ cells. Next, cells were centrifuged at 300g for 5 minutes, resuspended in 500µL of FACS Buffer, and transferred in FACS tubes through a 40µM strainer. The sorting was performed using BD FACSMelody sorter and the obtained BM cKit⁺ Lin⁻ cells were collected into 1.5mL DNA LoBind Eppendorf tubes (Epi-tubes) containing 200µL of FACS Buffer. The samples were then centrifuged at 1000g for 10 minutes at 4°C and after discarding the supernatant, cell pellets containing cKit⁺Lin⁻ cells were stored in a -80°C freezer until used for DNA extraction and 5-hmC measurement.

6. TET2 functional assay

To extract genomic DNA (gDNA) from cKit⁺ cells, a Monarch gDNA Purification Kit was used according to the manufacturer's protocol (New England Biolabs). To estimate the concentration of obtained gDNA, 1x dsDNA HS Assay Kit (Thermo Fisher Scientific) was used and the measurements were performed with the Qubit 4 Fluorometer (Thermo Fisher Scientific). To determine 5-hmC levels in cKit⁺ cells, a MethylFlash Hydroxymethylated DNA Fluorescence Quantification Kit was used according to the manufacturer's protocol (Epigentek), and the fluorescent signal was detected with an EnsSpire 2300 Multimode Plate Reader (PerkinElmer).

7. Liver tissue analysis

To determine the abundance of adipocytes in the liver, liver samples from mice were collected and prepared by fixing samples in 10% formalin overnight and then placed in cassettes for paraffin embedding. Afterward, samples were given to the Monash Department of Anatomy and Developmental Biology for hematoxylin staining (H&E) and imaging. Analysis was performed using Fiji Software.

8. Statistical analysis

All data are expressed as the mean ± SEM and were analyzed using two—way ANOVA or Student t test. P<0.05 was considered to be significant. All tests were performed using the Prism software (GraphPad Software, Inc., La Jolla, CA).

Results

DNMT3A^{+/R878H} mutation further increases body weight and fat content when fed a HFD

To mimic the scenario of clinical DNMT3A CHIP, irradiated CD45.1 recipient mice were first transplanted with donor BM cells consisting of either 10% CD45.2 DNMT3A^{+/+} or 10% CD45.2 DNMT3A^{+/R878H} BM cells, mixed with 90% of CD45.1 donor BM cells. The use of CD45.2 BM cells allows the tracking of clonal outgrowth of DNMT3A^{+/R878H} against CD45.1 WT BM cells. After 8 weeks of BM reconstitution where the immune system was replenished with either 90% WT/10% DNMT3A^{+/R878H} (DNMT3A CHIP) or 90% WT/10% DNMT3A^{+/+} (control) haematopoietic cells, both groups were placed on either a chow diet or HFD for 16 weeks. To confirm our HFD feeding period indeed induced obesity by increasing the overall body fat content, mice placed on either HFD or chow diet were subjected to body composition analysis using EchoMRI every 4 weeks for 16 weeks. The total body weight, as well as fat mass, significantly increased in both obese control and DNMT3A CHIP groups compared to their respective lean groups starting from week 8 (Figure 4A, B). As expected, the lean body mass, remained stable in all mice throughout the whole study period (Figure 4C), suggesting that overall weight gain occurred as a result of fat mass gain. Interestingly, obese DNMT3A CHIP mice revealed a greater weight increase compared to the obese control group. Although fat mass tended to increase further in obese DNMT3A CHIP mice, this was not statistically significant. This data revealed that obesity induces fat accumulation, and could perhaps be further exacerbated with DNMT3A mutation.

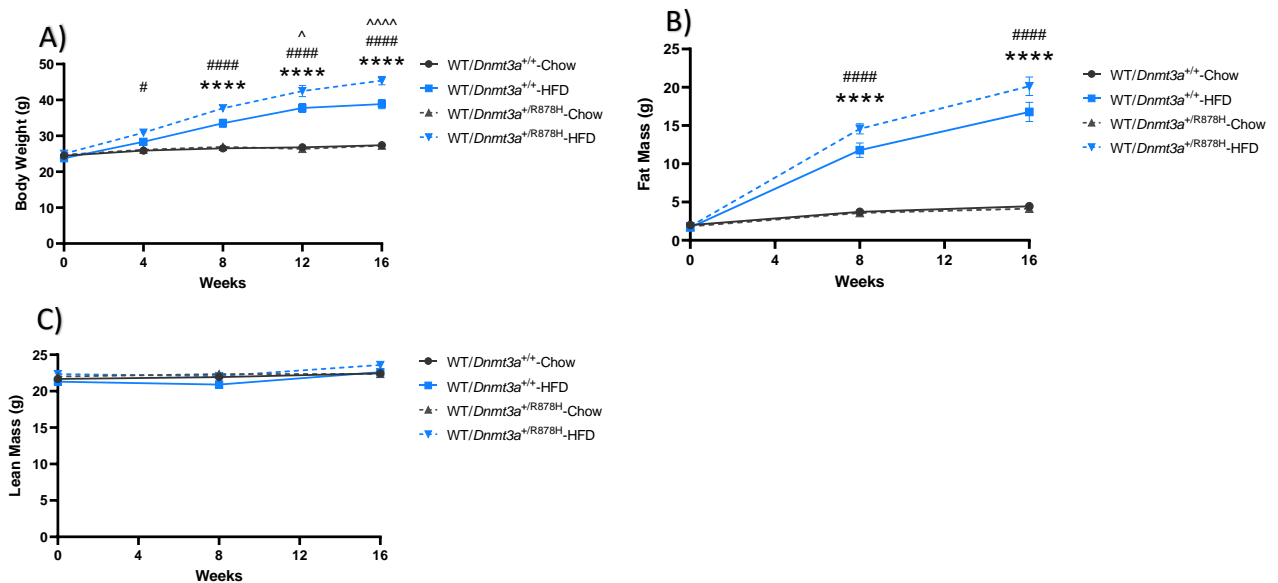


Figure 4. Obesity promoted a dramatic increase in body weight and fat mass in control and DNMT3A CHIP mice. (A) Body weight, (B) Fat Mass, and (C) Lean Mass of WT/DNMT3A^{+/+} and WT/DNMT3A^{+/R878H} lean and obese mice during 16 weeks of the experiment. $n = 10-12$. All data represent the mean \pm SEM. P values were obtained using a three-way ANOVA (multiple comparisons). */#/^ $P < 0.05$, ** $P < 0.01$, *** $P < 0.001$, **** $P < 0.0001$. “*” represents comparison between WT/DNMT3A^{+/+} Chow and WT/DNMT3A^{+/+} HFD; “#” represents comparison between WT/DNMT3A^{+/R878H} Chow and WT/DNMT3A^{+/R878H} HFD; “^” represents comparison between WT/DNMT3A^{+/+} HFD and WT/DNMT3A^{+/R878H} HFD.

High-fat diet accelerates myelopoiesis in WT/DNMT3A^{+R878H} mice

Next, we used flow cytometry to determine whether a HFD altered the abundance of monocytes in the blood of control and DNMT3A CHIP mice (**Figure 5**). A significant increase was observed in the total blood monocytes in both control and DNMT3A CHIP groups on a HFD, suggesting that obesity accelerates monocytosis regardless of whether mice had CHIP or not (**Figure 5A**). The clonal expansion of CD45.2 donor-derived monocytes was the most progressive in the obese DNMT3A CHIP mice and it was significantly increased compared to the lean DNMT3A CHIP and obese control groups (**Figure 5B**). This data shows that mice carrying DNMT3A^{+R878H} mutation are more prone to monocytic skewing in the setting of obesity.

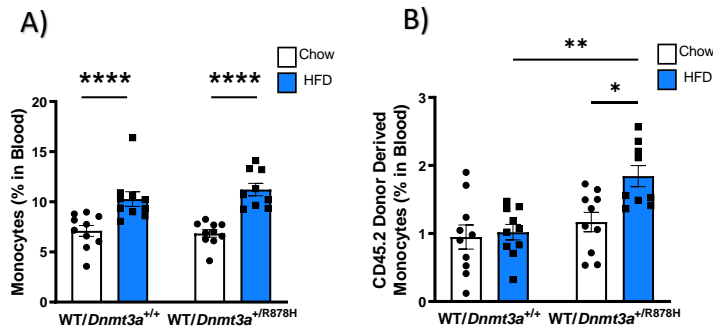


Figure 5. Obesity induces monocytosis in DNMT3A CHIP mice. WT/DNMT3A^{+/+} and WT/DNMT3A^{+R878H} mice were kept on chow or high-fat diet (HFD) for 16 weeks and flow cytometry was used to measure the (A) total monocyte and (B) CD45.2 donor-derived monocyte in the blood. $n = 10-12$. All data represent the mean \pm SEM. P values were obtained using a two-way ANOVA (multiple comparisons). * $p < 0.05$, ** $p < 0.01$, *** $p < 0.001$, **** $p < 0.0001$.

To further investigate the mechanism behind pronounced monocytosis in DNMT3A CHIP mice, the BM was harvested at week 16 and the abundance of CD45.2⁺ monocyte precursor cells such as HSCs, common myeloid progenitors (CMPs) and granulocyte-monocyte progenitors (GMPs) were measured. An increase in BM HSCs and CMPs was only observed in obese DNMT3A CHIP mice whereas GMPs were considerably elevated in both lean and obese DNMT3A CHIP groups (**Figure 6A-C**). The fact that the control group was relatively unaffected by the diet type suggests that DNMT3A^{+R878H} mutation can be a critical condition for enhanced myelopoiesis rather than obesity alone. Collectively, this data provides evidence that DNMT3A^{+R878H} has the potential to drive myelopoiesis that is further accelerated by obesity.

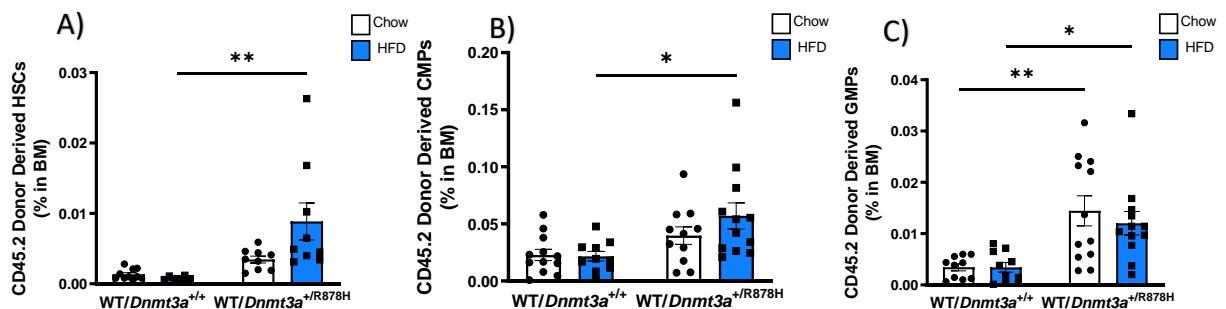


Figure 6. DNMT3A mutation has the potential to induce myelopoiesis. WT/DNMT3A^{+/+} and WT/DNMT3A^{+R878H} mice were kept on chow or high-fat diet (HFD) for 16 weeks and then humanely euthanized. Subsequently, the BM was harvested and flow cytometry was used to measure the levels of CD45.2 donor-derived (A) hematopoietic stem cells (HSCs), (B) common myeloid

progenitors (CMPs), and (C) granulocyte-monocyte progenitors (GMPs). $n = 10-12$. All data represent the mean \pm SEM. P values were obtained using a two-way ANOVA (multiple comparisons). * $p < 0.05$, ** $p < 0.01$.

High-fat diet accelerates liver fat and macrophage content in WT/DNMT3A^{+R878H} mice

Previously our lab and others have shown that a HFD increases the accumulation of fat in the liver as well as inflammatory macrophages due to increased monocyte infiltration. Therefore, after 16 weeks of HFD feeding, we also collected the liver to measure macrophage content and fat accumulation. By embedding and fixing liver tissues for sectioning and H&E staining, we observed a significant increase in lipid abundance with a HFD. Interestingly, we found that HFD-fed DNMT3A CHIP mice had further increased lipid content compared to HFD-fed control mice (**Figure 7A, B**). Next, we used flow cytometry to measure macrophage content in the liver. Consistent with our blood monocyte data we observed a significant increase in total macrophages in both HFD-fed groups (**Figure 7C**) and more importantly, obese DNMT3A CHIP mice had a further increase in donor-derived CD45.2 macrophage subset (**Figure 7D**). These findings altogether confirm that obesity has an inflammatory nature and in the presence of DNMT3A mutation, it further accelerates lipid accumulation and inflammation.

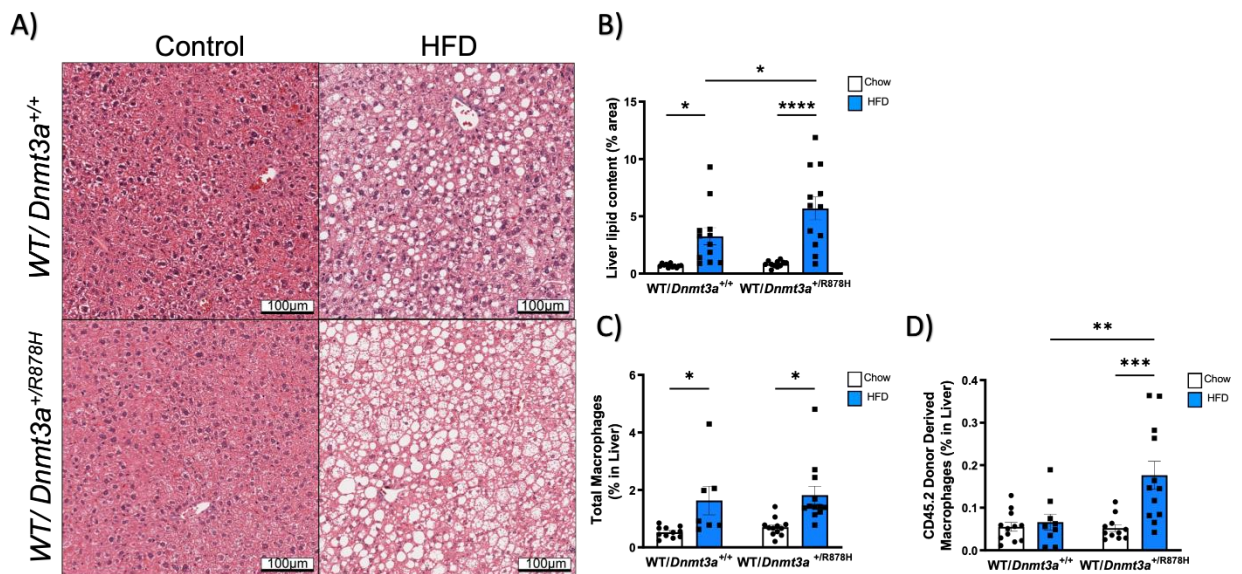


Figure 7. DNMT3A CHIP obese mice represent increased lipid content and CD45.2 donor-derived macrophages in the liver. WT/DNMT3A^{+/+} and WT/DNMT3A^{+/R878H} mice were kept on a chow or high-fat diet (HFD) for 16 weeks and then humanely euthanized. Subsequently, liver samples were harvested and (A) liver tissues were analysed by staining and imaging liver tissue slides. (B) The lipid-covered liver area (shown as white vesicles) was further calculated in percentages. Flow cytometry was used to measure the (C) total macrophages and (D) CD45.2 donor-derived macrophages in the liver. $n = 9-12$. All data represent the mean \pm SEM. P values were obtained using a two-way ANOVA (multiple comparisons). * $p < 0.05$, ** $p < 0.01$, *** $p < 0.001$.

Obesity reduces TET2 activity in bone marrow HSCs

Recently it was discovered that diabetes, another metabolic disease, exacerbated myelopoiesis through the dysregulation of an AMPK-TET2 pathway in BM HSCs³⁶. Since obesity-induced inflammation is a known AMPK suppressor, we postulated that obesity could perhaps also promote myeloid skewing in BM HSCs through the dysregulation of the AMPK-TET2 axis. To test this, CD45.2⁺ cKit⁺ lineage-committed cells (CD45.2⁺ HSCs) from the BM harvested at week 16

from obese and lean control and DNMT3A CHIP mice were sorted using fluorescent-activated cell sorting (FACS) and then measured for TET2 activity. Since TET2 catalyzes DNA 5-cytosine hydroxymethylation (5-hmC), the TET2 activity was measured through 5-hmC levels quantification. As observed, both DNMT3A CHIP and control obese mice significantly decreased their 5-hmC levels in CD45.2⁺ HSCs compared to lean mice, suggesting that TET2 activity was indeed reduced (**Figure 8**).

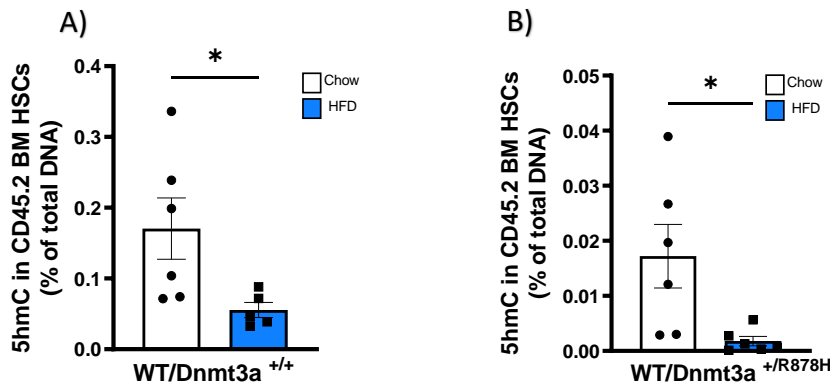


Figure 8. Obesity results in the reduction of 5-hmC in BM HSCs of both control and DNMT3A CHIP mice. The percentage of DNA 5-cytosine hydroxymethylation (5-hmC) of CD45.2 donor-derived BM HSCs was measured in (A) WT/DNMT3A^{+/-} and (B) WT/DNMT3A^{+/-R878H} experimental groups kept on either chow and HFD. n=6. All data represent the mean ± SEM. P values were obtained using a t-test. *p < 0.05.

AMPK activator O-304 reduces HFD-induced body weight and fat mass, and blood monocytes

To determine if AMPK activator O-304 could be used to reduce DNMT3A CHIP-induced myeloid expansion in the setting of obesity, BMT was again performed into CD45.1 recipient mice consisting of BM cells of 10% CD45.2 DNMT3A^{+/-R878H} with 90% CD45.1 WT cells. After 8 weeks of reconstitution to replenish the immune system with 90% WT and 10% DNMT3A^{+/-R878H} haematopoietic cells, mice were placed on a HFD with or without the AMPK activator O-304 supplemented in their diet for 16 weeks while their body composition and monocyte levels in the blood were measured every 4 weeks. Since the study is still ongoing, data is only captured until the week 8 timepoint for this paper. As observed, the O-304 treated group indeed reduced total body weight (**Figure 9A**) and fat mass (**Figure 9B**) at the 4 and 8-week timepoint, whereas lean mass remained unchanged as expected (**Figure 9C**). This suggests that O-304 prevented fat accumulation in DNMT3A CHIP mice on a HFD.

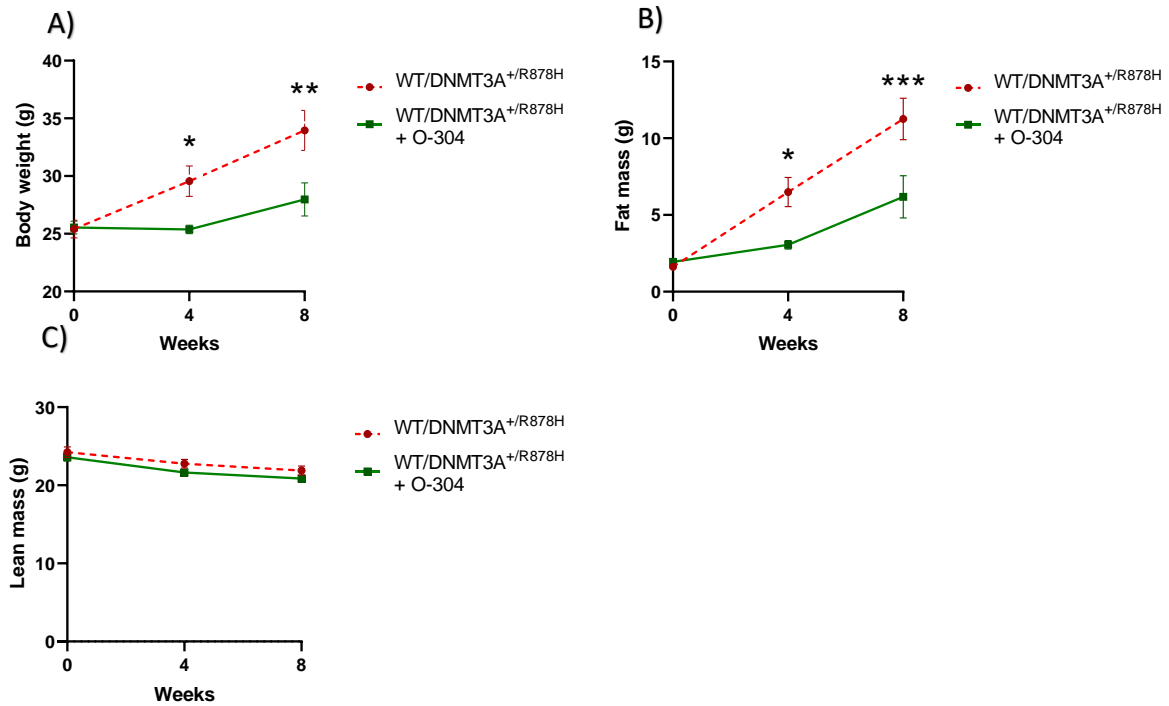


Figure 9. AMPK activator O-304 reduces fat accumulation in obese DNMT3A CHIP mice. (A) Body weight, (B) Fat Mass, and (C) Lean mass of WT/DNMT3A^{+/R878H} mice on HFD with or without O-304 during 8 weeks of the experiment. *n* = 7-9. All data represent the mean ± SEM. *P* values were obtained using a three-way ANOVA (multiple comparisons). **p* < 0.05, ***p* < 0.01, ****p* < 0.001.

Finally, to investigate whether O-304 could reduce the abundance of monocytes in the blood in DNMT3A CHIP mice on a HFD we measured monocyte abundance in the blood at the week 8 timepoint. Despite observing early changes in body weight and fat mass at week 8 timepoint, we found no significant difference in monocyte levels in the blood at 8 weeks of O-304 treatment. (Figure 10). Moreover, when we measured the CD45.2 donor-derived fraction of monocytes that contained DNMT3A^{+/R878H} mutation, we also found no significant difference between the HFD and HFD + O-304 groups. However, as this study is still ongoing, it does not represent the final results as we only observed significant increases in monocytes after 16 weeks of HFD feeding.

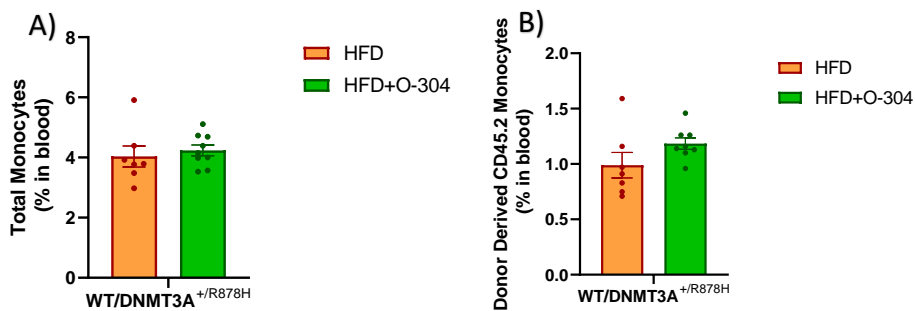


Figure 10. AMPK activator O-304 does not change monocyte levels in obese DNMT3A CHIP mice at week 8. WT/Dnmt3a^{+/R878H} mice were kept on a high-fat diet (HFD) with or without O-304 for 8 weeks and flow cytometry was used to measure the (A) total monocyte and (B) CD45.2 donor-derived monocyte in the blood. *n* = 7-9. All data represent the mean ± SEM. *P* values were obtained using an unpaired *t*-test.

Discussion

Although CHIP is a common age-related premalignant state, the majority of CHIP patients' mortality cases are associated with CVD development rather than cancer^{2,10}. Obesity is one of the major contributors to CVD progression and according to recent studies, the outgrowth of hematopoietic clones with *DNMT3A* mutation is accelerated in obese patients. However, the underlying mechanism that links obesity and CHIP is still largely unknown^{29,32}.

In the current study, we used a murine model of obesity with *DNMT3A* mutation and discovered that these mice had increased clonal expansion of monocytes in the blood compared to obese mice that did not have the mutation. Moreover, we found that the clonal expansion of monocytes was due to enhanced myelopoiesis in the BM. Interestingly, the clonal outgrowth of monocytes due to *DNMT3A* mutation was associated with increased macrophages in the liver, accompanied by increased lipid accumulation in the liver of *DNMT3A* CHIP obese mice. These data corroborate with earlier findings from Nagareddy et al, where they observed an increase in myelopoiesis and circulating monocytes when mice were placed on a HFD²⁹. Mechanistically, they found that macrophages recruited into lipid-containing tissues by local inflammatory cytokines are further upregulated to express and secrete IL-1 β which directly facilitates myeloid skewing in BM³⁴. Whether or not IL-1 β could be responsible for the clonal expansion of monocytes during HFD feeding in *DNMT3A* CHIP mice was not explored in the current study.

Surprisingly, we also found that *DNMT3A* mutation played a role in whole-body metabolism by further increasing body weight and fat mass compared to obese mice that had no mutation. This observation suggests that *DNMT3A* mutation in only haematopoietic cells can also have extrinsic roles in affecting non-haematopoietic tissues. Interestingly, these findings are in line with a study from Tovy et al. where they showed similar effects on whole-body metabolism in human Tatton-brown Rahman syndrome (TBRS), also known as *DNMT3A* overgrowth syndrome with a partial or complete loss of *DNMT3A*³⁷. Although TBRS is different from our *DNMT3A*-driven CHIP model with only 10% of the BM consisting of *DNMT3A*^{+/*R878H*}, it does suggest that this small proportion of cells can clonally expand and contribute to changes in whole-body metabolism. In future experiments, it will be interesting to understand in more detail the mechanism behind *DNMT3A* mutation-induced whole-body metabolism dysfunction.

Recently, our laboratory demonstrated that diabetes, another metabolic disease, exacerbated the clonal expansion of monocytes via increased myelopoiesis. Mechanistically, this was due to a reduction in AMPK activity in HSCs, which led to a reduction in TET2 activity. As obesity is a known suppressor of AMPK, we used an AMPK activator, O-304, to explore whether myelopoiesis and increased circulating monocytes could be reversed³⁴. Unfortunately, as this study is still ongoing, we found no reduction in clonal outgrowth in circulating monocytes in *DNMT3A* CHIP mice for the 8-week feeding period. However, we did observe a significant reduction in body weight and fat mass in *DNMT3A* CHIP obese mice compared to control obese mice early on after 4 weeks of HFD feeding. As O-304 was administered systemically, O-304 may have affected whole-body metabolism directly rather than acting on myelopoiesis-induced inflammation.

Nevertheless, the 5-hmC levels in HSCs in the obese mice were seen to be significantly reduced, suggesting that obesity may suppress the functioning of the AMPK-TET2 pathway. Although obesity is known to suppress AMPK it cannot be confirmed whether it was AMPK dysfunction or excess IL-1 β that promoted an aberrant myelopoiesis as previously mentioned. In this respect,

for future studies, profiling IL-1 β levels as well as other inflammatory cytokines in BM is important to explore the true importance of AMPK and inflammation in this process. Secondly, we did not verify if AMPK was indeed reduced by obesity. Although the previous studies already demonstrated the link between AMPK and obesity, to eliminate the limitations of this study, it is important to measure the levels of active AMPK in HSCs (phosphorylated AMPK)^{29,30}. More importantly, as at the time of this paper, there are still 8 weeks of HFD feeding and therefore the cellular effect of O-304 on myelopoiesis and monocytes in the blood is yet to be truly assessed at 16 weeks, in which we observed increased monocytes with *DNMT3A* mutation.

Conclusion

Collectively, this study demonstrated that obesity accelerated *DNMT3A* myeloid outgrowth possibly through the dysfunction of the AMPK-TET2 pathway. We also observed an increase in body weight and fat mass in *DNMT3A* CHIP obese mice compared to control obese mice. Finally, when we administered AMPK activator O-304, body weight, and fat mass significantly reduced while circulating monocytes were unchanged at 8 weeks of HFD feeding so far.

References

1. Mooney, L. G. (2021). Clonal haematopoiesis of indeterminate potential: intersections between inflammation, vascular disease and heart failure. *Clinical science (London, England: 1979)*, *135*(7), 991-1007.
2. Jaiswal, S. e. (2017). Clonal Hematopoiesis and Risk of Atherosclerotic Cardiovascular Disease. *The New England journal of medicine*, *377*(2), 111–121.
3. van Deuren, R. C. et al (2021). Expansion of mutation-driven haematopoietic clones is associated with insulin resistance and low HDL-cholesterol in individuals with obesity.
4. Libby, P. et al (2019). Clonal Hematopoiesis: Crossroads of Aging, Cardiovascular Disease, and Cancer: JACC Review Topic of the Week. *Journal of the American College of Cardiology*, *74*(4), 567–577.
5. Kandarakov, O., & Belyavsky, A. (2020). Clonal Hematopoiesis, Cardiovascular Diseases and Hematopoietic Stem Cells. *International journal of molecular sciences*, *21*(21), 7902.
6. Abegunde, S. O., Buckstein, R., Wells, R. A., & Rauh, M. J. (2018). An inflammatory environment containing TNF α favors Tet2-mutant clonal hematopoiesis. *Experimental Hematology*, *59*, 60–65.
7. Beerman I. (2017). Accumulation of DNA damage in the aged hematopoietic stem cell compartment. *Seminars in hematology*, *54*(1), 12–18.
8. Genovese, G. et al. (2014). Clonal hematopoiesis and blood-cancer risk inferred from blood DNA sequence. *The New England journal of medicine*, *371*(26), 2477–2487.
9. Steensma D. P. (2018). Clinical consequences of clonal hematopoiesis of indeterminate potential. Hematology. American Society of Hematology. *Education Program*, *2018*(1), 264–269.
10. Jaiswal, S. et al. (2014). Age-related clonal hematopoiesis associated with adverse outcomes. *The New England journal of medicine*, *371*(26), 2488–2498.
11. Zink, F. et al (2017). Clonal hematopoiesis, with and without candidate driver mutations, is common in the elderly. *Blood*, *130*(6), 742–752.
12. Challen, G. A. et al (2011). Dnmt3a is essential for hematopoietic stem cell differentiation. *Nature genetics*, *44*(1), 23–31.
13. Murphy, A.J., Dragoljevic, D., Natarajan, P., & Wang, N. (2022). Hematopoiesis of Indeterminate Potential and Atherothrombotic Risk. *Thrombosis and Haemostasis*, *122*, 1435 - 1442.
14. Chambers, S. M. et al (2007). Hematopoietic fingerprints: an expression database of stem cells and their progeny. *Cell stem cell*, *1*(5), 578–591.
15. Zhang, X. et al (2016). DNMT3A and TET2 compete and cooperate to repress lineage-specific transcription factors in hematopoietic stem cells. *Nature genetics*, *48*(9), 1014–1023.
16. Ito, K. et al (2019). Non-catalytic Roles of Tet2 Are Essential to Regulate Hematopoietic Stem and Progenitor Cell Homeostasis. *Cell reports*, *28*(10), 2480–2490.e4.
17. Sandoval, J. E., Huang, Y. H., Muise, A., Goodell, M. A., & Reich, N. O. (2019). Mutations in the DNMT3A DNA methyltransferase in acute myeloid leukemia patients cause both loss

- and gain of function and differential regulation by protein partners. *The Journal of biological chemistry*, 294(13), 4898–4910.
18. Moran-Crusio, K. et al (2011). Tet2 Loss Leads to Increased Hematopoietic Stem Cell Self-Renewal and Myeloid Transformation. *Cancer Cell*, 20(1), 11–24.
 19. Abdel-Wahab, O. et al (2009). Genetic characterization of TET1, TET2, and TET3 alterations in myeloid malignancies. *Blood*, 114(1), 144–147.
 20. Fuster, J. J. et al (2017). Clonal hematopoiesis associated with TET2 deficiency accelerates atherosclerosis development in mice. *Science (New York, N.Y.)*, 355(6327), 842–847.
 21. Challen, G. A. et al (2011). Dnmt3a is essential for hematopoietic stem cell differentiation. *Nature genetics*, 44(1), 23–31.
 22. Jeong, M. et al (2018). Loss of Dnmt3a Immortalizes Hematopoietic Stem Cells In Vivo. *Cell reports*, 23(1), 1–10.
 23. Cole, C. B. et al (2017). Haploinsufficiency for DNA methyltransferase 3A predisposes hematopoietic cells to myeloid malignancies. *The Journal of clinical investigation*, 127(10), 3657–3674.
 24. Sano, S., Oshima, K., Wang, Y., Katanasaka, Y., Sano, M., & Walsh, K. (2018). CRISPR-Mediated Gene Editing to Assess the Roles of Tet2 and Dnmt3a in Clonal Hematopoiesis and Cardiovascular Disease. *Circulation research*, 123(3), 335–341.
 25. Guo, L. Y., Yang, F., Peng, L. J., Li, Y. B., & Wang, A. P. (2020). CXCL2, a new critical factor and therapeutic target for cardiovascular diseases. *Clinical and experimental hypertension (New York, N.Y.: 1993)*, 42(5), 428–437.
 26. Xu, Y., Murphy, A. J., & Fleetwood, A. J. (2022). Hematopoietic Progenitors and the Bone Marrow Niche Shape the Inflammatory Response and Contribute to Chronic Disease. *International journal of molecular sciences*, 23(4), 2234.
 27. Nagareddy, P. R. et al (2013). Hyperglycemia promotes myelopoiesis and impairs the resolution of atherosclerosis. *Cell metabolism*, 17(5), 695–708.
 28. Powell-Wiley, T. M. et al (2021). Obesity and Cardiovascular Disease: A Scientific Statement From the American Heart Association. *Circulation*, 143(21), e984–e1010.
 29. Nagareddy, P. R. et al (2014). Adipose tissue macrophages promote myelopoiesis and monocytosis in obesity. *Cell metabolism*, 19(5), 821–835.
 30. Murray, Peter J. (2014). Obesity Corrupts Myelopoiesis. *Cell Metabolism*, 19(5), 735–736.
 31. Weisberg, S. P., McCann, D., Desai, M., Rosenbaum, M., Leibel, R. L., & Ferrante, A. W., Jr (2003). Obesity is associated with macrophage accumulation in adipose tissue. *The Journal of clinical investigation*, 112(12), 1796–1808.
 32. van Deuren, R. C. et al (2021). Expansion of mutation-driven haematopoietic clones is associated with insulin resistance and low HDL-cholesterol in individuals with obesity.
 33. Jeon S. M. (2016). Regulation and function of AMPK in physiology and diseases. *Experimental & molecular medicine*, 48(7), e245.
 34. Gauthier, M. S. et al (2011). Decreased AMP-activated protein kinase activity is associated with increased inflammation in visceral adipose tissue and with whole-body insulin resistance in morbidly obese humans. *Biochemical and biophysical research communications*, 404(1), 382–387.

35. Zhang, T. et al (2019). Phosphorylation of TET2 by AMPK is indispensable in myogenic differentiation. *Epigenetics & chromatin*, 12(1), 32.
36. Wu, D., et al (2018). Glucose-regulated phosphorylation of TET2 by AMPK reveals a pathway linking diabetes to cancer. *Nature*, 559(7715), 637–641
37. Tovy, A. et al (2022). Constitutive loss of DNMT3A causes morbid obesity through misregulation of adipogenesis. *eLife*, 11, e72359.

Appendix

Supplementary table

Table S1. Key Reagents Table

| Reagent | Source | Identification code |
|--|--------------|---------------------|
| <i>Mouse strain</i> | | |
| Recipient Ly5.1 (CD45.1) | SVI | N/A |
| Donor Ly5.1 (CD45.1) DNMT3A ^{+/+} | SVI | N/A |
| Donor Ly5.2 (CD45.2) DNMT3A ^{+/R878H} | SVI | N/A |
| <i>Flow antibodies</i> | | |
| Pacific Blue™ anti-mouse CD45 Antibody (clone: 30-F11) | BioLegend | Cat#103126 |
| PerCP-cytm 5.5 rat anti-mouse Ly-6G/Ly-6C (gr-1) Antibody (clone: RB6-8C5) | BD Sciences | Cat#552093 |
| Brilliant Violet 605™ anti-mouse CD115 Antibody (clone: RB6-8C5) | BioLegend | Cat#135517 |
| PE anti-mouse CD3 Antibody (clone 17A2) | BioLegend | Cat#100206 |
| FITC anti-mouse CD8a Antibody (clone: 53-6.7) | Invitrogen | Ref#11-0081-85 |
| BUV496 anti-mouse CD4 Antibody (clone: GK1.5) | BD Sciences | Cat#612952 |
| APC anti-mouse/human CD45R/B220 Antibody (clone: RA3-6B2) | BioLegend | Cat#103212 |
| Alexa Fluor 700 anti-mouse CD45.2 Antibody (clone: 104) | BioLegend | Cat#109822 |
| PE/Cyanine7 anti-mouse CD45.1 Antibody (clone: A20) | BioLegend | Cat#110730 |
| FITC anti-mouse CD3 Antibody (clone: 500A2) | BioLegend | Cat#152304 |
| FITC anti-mouse/human CD11b Antibody (clone: M1/70) | BioLegend | Cat#101206 |
| FITC anti-mouse Ly-6G/Ly-6C (Gr-1) Antibody (clone: RB6-8C5) | BioLegend | Cat#108406 |
| FITC anti-mouse CD19 Antibody (clone: MB19-1) | ThermoFisher | Ref#11-0191-85 |
| FITC anti-mouse CD4 Antibody (clone: RM4-5) | BioLegend | Cat#100510 |
| FITC anti-mouse TER-119/Erythroid Cells Antibody (clone: TER-119) | BioLegend | Cat#116206 |
| FITC anti-mouse/human CD45R/B220 Antibody (clone: RA3-6B2) | Invitrogen | Ref#11-0452-85 |
| FITC anti-mouse CD2 Antibody (clone: RM2-5) | BioLegend | Cat#100105 |
| APC/Cyanine7 anti-mouse CD117 (c-kit) Antibody (clone: 2B8) | BioLegend | Cat#105826 |
| Pacific Blue™ anti-mouse Ly-6A/E (Sca-1) Antibody | BioLegend | Cat#108120 |

(clone: D7)

PerCP/Cyanine5.5 anti-mouse CD64 (Fc γ RI)
Antibody

BioLegend

Cat#139207

(clone: X54-5/7.1)

APC anti-mouse CD34

BioLegend

Cat#128611

(clone: HM34)

PE/Cyanine7 anti-mouse F4/80

BioLegend

Cat# 123113

(clone: BM8)

Supplementary figures

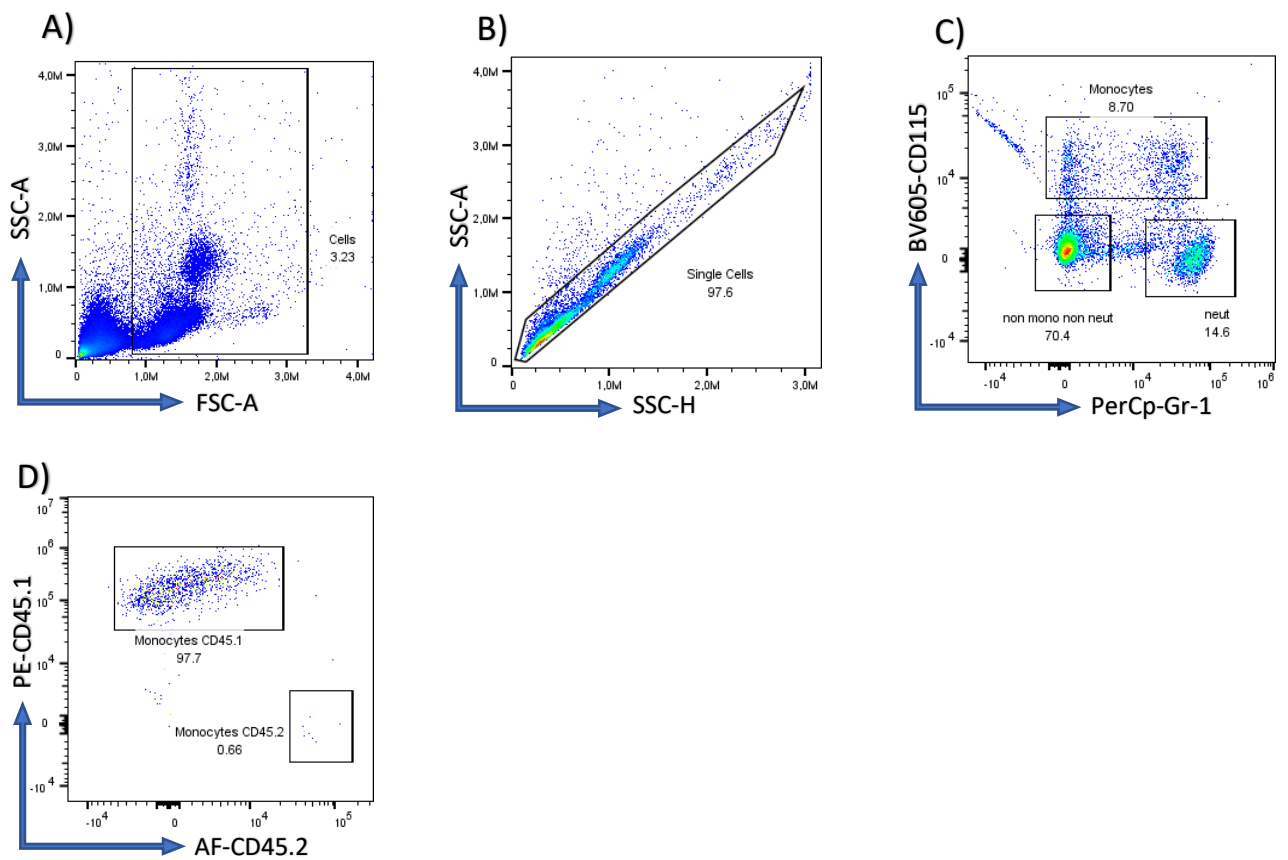


Figure S1. Gating strategy for mouse blood leukocytes. (A) The side scatter area (SSC-A) vs. forward scatter area (FSC-A) graph was used to gate all living cells. (B) SSC-A vs. side scatter height (SSC-H) graph was used to gate single cells. (C) From the single cell population, CD115 vs. Gr-1 graph was used to gate monocytes, neutrophils, and non-myeloid cells. (D) From total monocytes, PE-CD45.1 vs. AF-CD45.2 plot was used to differentiate between CD45.1⁺ and CD45.2⁺ populations.

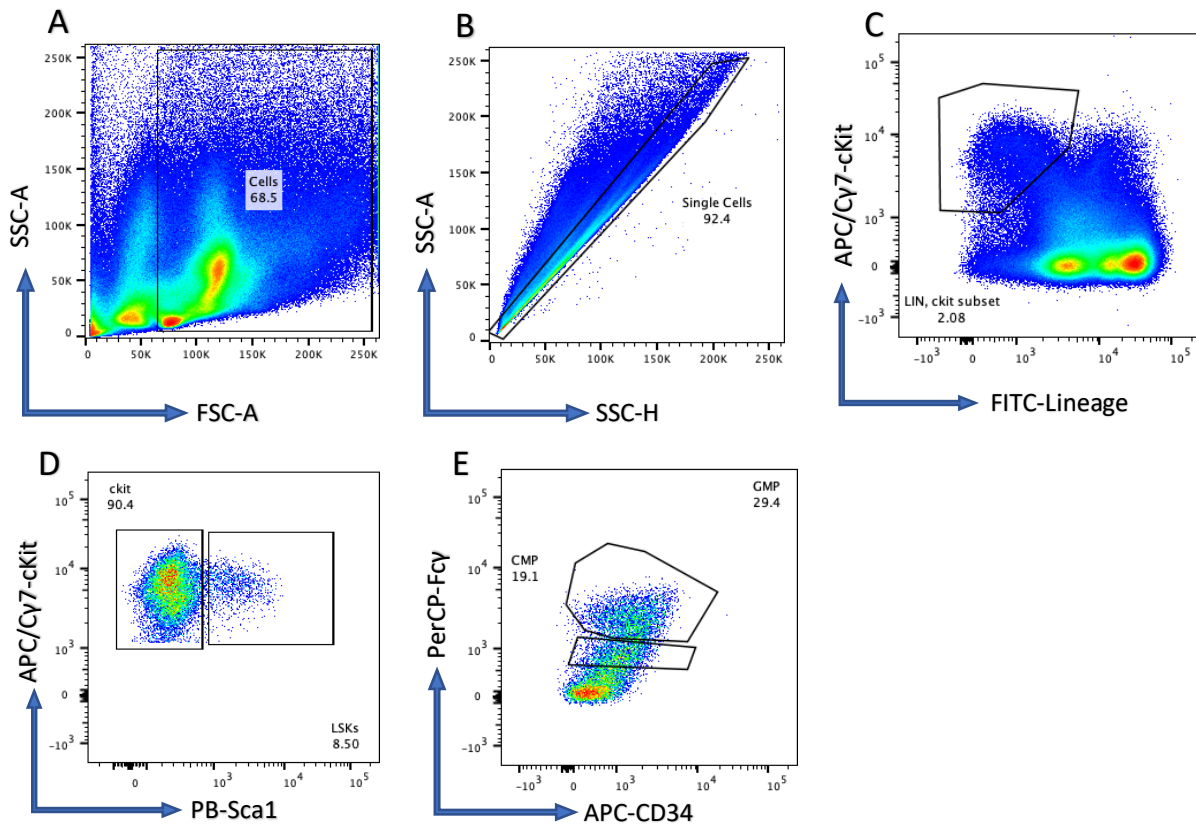


Figure S2. Gating strategy for mouse bone marrow cells. (A) The side scatter area (SSC-A) vs. forward scatter area (FSC-A) graph was used to gate all living cells. (B) SSC-A vs. side scatter height (SSC-H) graph was used to gate single cells. (C) On $cKit^+$ vs. lineage graph, $Lin^- cKit^+$ cells were gated. (D) From the $Lin^- cKit^+$ population, $cKit$ vs. $Sca1$ graph was used to gate $Sca1^+$ LSKs (HSCs) from $Sca1^- cKit^+$ subset (HPCs). (E) From $Sca1^- cKit^+$ cells, Fcy vs. $CD34$ graph was used to gate CMPs and GMPs. HSCs, CMPs, and GMPs were divided into $CD45.1^+$ and $CD45.2^+$ in a similar manner as monocytes (see Figure S1).